

Microtomography of Systems at High Pressure I: Microtomography of Recovered Products from Fe-rich Melt Segregation Run

T. Uchida, Y. Wang, M.L. Rivers, S.R. Sutton, F. Westferro, J. Gebhardt
Consortium for Advanced Radiation Sources, The University of Chicago, Chicago, IL, U.S.A.

Introduction

We have been developing techniques for synchrotron microtomographic imaging under high pressure and temperature to allow *in situ* microstructural observations. In the present study, we report on the results obtained from *in situ* high-pressure experiments on samples containing Fe-alloy melt in the presence of mantle minerals with microtomography and electron microprobe analyses on recovered run products. The results show the potential of high-pressure tomographic experiments.

Methods and Materials

High-pressure experiments have been performed by using the 250-ton cubic anvil press installed at the sector 13 bending magnet beamline at the APS. Schematics of the sample assembly are shown in Fig. 1. A 9-mm edge-length pyrophyllite cube was compressed by anvils with 6-mm truncations. The sample was encapsulated by hexagonal boron nitride and heated by a graphite tube heater. The temperature was measured by a thermocouple, while the pressure was determined from the lattice strains in a gold (Au) pressure standard by using the equation of state [1]. Two different series of high-pressure experiments on an Fe-rich melt were carried out: (1) Fe segregation experiments, in which Fe alloy was uniformly mixed with

different light elements (S, H, C, and Si) and minerals (MgSiO_4 , MgSiO_3 , and MgO), and (2) Fe migration experiments, in which the Fe alloy was placed in powdered mantle minerals as an embedded inclusion.

After the high-pressure experiments, the spatial and size distribution of iron droplets in the recovered samples were observed by using microtomography [2] (Fig. 2). The data were collected at the same experimental station (13-BM-D). The energy of the monochromatic x-ray beam was 45 keV, which was optimized to obtain good contrast between the Fe-rich melt and surrounding mantle minerals. The transmitted x-rays were imaged with a single-crystal yttrium-aluminum-garnet (YAG) scintillator (0.2-mm thick), a microscope objective, and a 1242×1152 -pixel fast charge-coupled device (CCD) detector. The field of view was approximately 3×3 mm, which resulted in a spatial resolution of about $4.0 \mu\text{m}$, after 2×2 binning. Over 720 x-ray projections were collected by rotating the sample through 180° . Then tomographic reconstructions were carried out by using filtered backprojection for all of the angles in a given row. The reconstructed volume data can be visualized as 2-D slices or 3-D movies.

Recovered run products were further examined by electron microprobe.

Results and Discussion

Figure 3 compares the images obtained for different stages of the melt migration process in the system Fe-S-MgO. In experiments where the Fe-S alloy inclusion was surrounded by MgO [Fig. 3(a) and 3(b)], the Fe-S alloy melt was distributed locally around the original position. At 1400K, the boundaries between the Fe-S alloy and MgO became rounded, indicating melting of the alloy [Fig. 3(a)], but the melt did not have much mobility, probably because the surrounding MgO was in the solid state. However, the MgO immediately adjacent to the alloy shows slightly brighter intensities than that in other areas in the tomographic image, suggesting higher density. When the temperature was further increased to 1600K, the Fe-S alloy formed a sphere because of its high surface tension, suggesting melting of adjacent MgO. At the same time, some intensity contrast in the spheres was also observed (indicated by the white arrow). On the other hand, when Fe-S was intimately mixed with MgO [Fig. 3(c)],

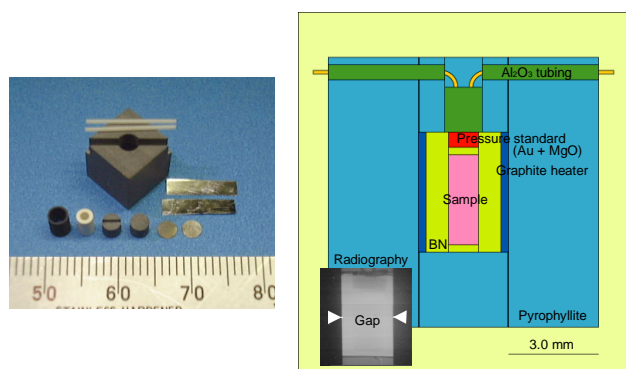


FIG. 1. Pyrophyllite cubes with a 9-mm edge length are employed as a pressure medium. Sample is surrounded by BN and heated by the outer graphite tube. The temperature is measured by a thermocouple, while the pressure is obtained from the strain in a pressure standard (Au).

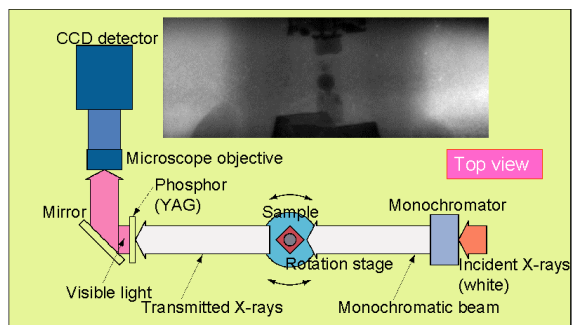


FIG. 2. Schematic showing the setup of computed microtomography. Transmitted x-rays are converted by the YAG single crystal to visible light, which is then reflected by the mirror through a microscope objective into the CCD detector. The inset is a radiograph from one of the Fe melt experiments.

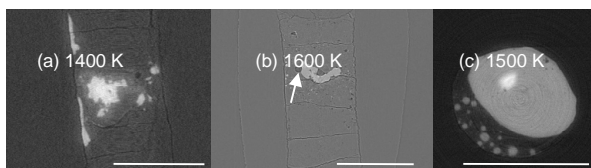


FIG. 3. Comparison of tomographic images in an Fe-S-MgO system. The samples were recovered from 4 GPa at (a) 1400K, (b) 1600K, and (c) 1500K. The white bar at the bottom of each image indicates 1 mm. (a) and (b) were embedded alloy inclusions, and (c) was mixed powder.

composition variation in the alloy was observed, in addition to bright and dark spheres. The difference in these experiments appears to depend on whether the Fe-S alloy is local or uniform; therefore, the activity of S may be the key. Chemical analysis with an electron probe is underway to address this issue.

In the system Fe-Si-MgSiO₃ (Fig. 4), halos are clearly observed around the spheres (indicated by the arrows). The temperature must be increased to 1600K to melt the alloy (higher than the system containing S). The recovered samples show a consistent texture, even though the initial sample configuration was different. These observations contrast with the results obtained in the system containing S. The alloy seems to react with the surrounding MgSiO₃ to form halos. The mechanism of forming the halo is the key point. Chemical analysis is in progress to determine the mechanism of halo formation.

Figure 5 shows a comparison of microtomography and electron microprobe analysis for the system containing S. The composition variation in the quenched Fe-S melt was identified as Fe_{0.60}S_{0.40} (Fe₃S₂) and Fe_{0.99}S_{0.01} by electron

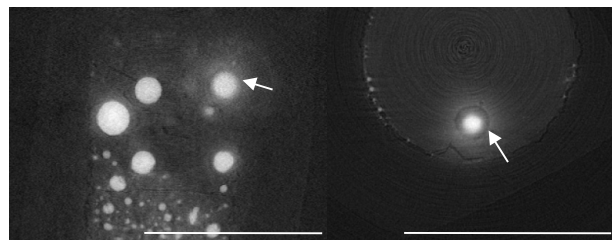


FIG. 4. Comparison of tomographic images in Fe-Si-MgSiO₃ system. Experiments were performed with FeSi (a) mixed with MgSiO₃ and (b) embedded in MgSiO₃. Both samples were recovered from 4 GPa and 1700K. The white bar indicates 1 mm.

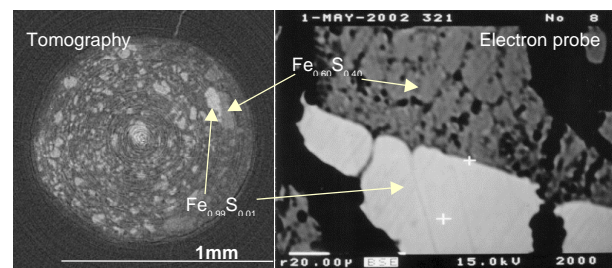


FIG. 5. Comparison of tomographic image and backscattered electron image. The contrast due to Fe content is clearly observed in both images.

probe analysis. This contrast in chemical composition is well-correlated to the intensity contrast in the reconstructed slices in microtomography. In principle, the tomographic images can be quantified in terms of chemical composition.

Acknowledgments

We thank N. Lazarz, F. Sopron, M. Jagger, G. Shen, V. Prakapenka, M. Newville, P. Eng, J. Pluth, and C. Pullins for their valuable contributions. Work performed at GSECARS is supported by the National Science Foundation (Earth Sciences), U.S. Department of Energy (DOE, Geosciences), W.M. Keck Foundation, and U.S. Department of Agriculture. Use of the APS was supported by the DOE Office of Science, Office of Basic Energy Sciences, under Contract No. W-31-109-ENG-38.

References

- [1] O.L. Anderson, D.G. Isaak, and S. Yamamoto, *J. Appl. Phys.* **65**, 1534-1543 (1989).
- [2] M.L. Rivers, S.R. Sutton, and P. Eng, in *Developments in X-ray Tomography II*, edited by U. Bonse (International Society for Optical Engineering, Bellingham, WA, 1999), pp. 78-86.